Tribology Online
Japanese Society of Tribologists

Tribology Online, 7, 1 (2012) 13-23.
ISSN 1881-2198
DOI 10.2474/trol.7.13

Article

Hydrodynamic Lubrication Effects of Multiple Circular Bump Pattern for a Thrust Sliding Bearing of a Scroll Compressor

Sanemasa Kawabata[1)*], Shigeki Iwanami [2)], Tadashi Hotta[2)], Fumihiro Itoigawa[3)] and Takashi Nakamura[3)]

[1)]Materials R&D Division, DENSO CORP.
[2)]Climate Cooling and Heating Engineering Division 2, DENSO CORP.
1-1 Showa, Kariya, Aichi 448-8661, Japan
[3)]Graduate School of Engineering, Nagoya Institute of Technology
Gokiso, Showa-ku, Nagoya 460-8555, Japan
*Corresponding author: sanemasa_kawabata@denso.co.jp

(Manuscript received 13 September 2011; accepted 26 December 2011; published 31 January 2012)

The optimum texturing pattern for a thrust sliding bearing of a scroll compressor was investigated. As the basis of lubrication analysis for multiple circular bumps pattern, fundamental hydrodynamic lubrication effects of the axisymmetric circular geometry expressed by the power law formula were analyzed using elastohydrodynamic lubrication (EHL) analysis. The optimum geometry to improve the load carrying capacity and reduce frictional force for the model geometry was discussed. Frictional properties of the proposed thrust bearings were experimentally evaluated and compared with numerically predicted properties. In order to clarify the robustness against accidental high load, seizure limits of a circular bump pattern were experimentally evaluated. These results show that the initial frictional properties are able to control by the crowning profile, the proposed pattern has a sufficiently low friction coefficient and quite a high seizure limits.

Keywords: elastohydrodynamic lubrication, circular bump, texture, thrust bearings, scroll compressor

1. Introduction

In scroll compressors, a thrust sliding bearing is used to support the orbiting scroll against the thrust force from compressed refrigerant in scroll chamber (Fig.1). A high load carrying capacity and low friction bearing is required especially for a CO_2 compressor due to its high refrigerant pressure. In conventional refrigerant systems, a simple flat plate has been used as the thrust bearing. Oku et al. [1,2] explained the lubrication mechanism by the effect of global wedge resulting from elastic deformation of the orbiting scroll, and proposed the optimum design criteria. The geometrical wedge profile plays a dominant role in oil pressure generation and sufficiently flat surface is required. For high operating pressure CO_2 systems, a hydrostatic thrust bearing is often used to ensure the high load carrying capacity. One of the disadvantages of the flat plate type thrust bearings was a lack of reproducibility in frictional performances. The scroll thrust bearing is rather a large scale bearing, and there are some difficulties of manufacture to keep the flatness and waviness level in desired range for the necessary frictional properties. The aim of this study is to achieve a sufficient lubrication performance using a textured thrust plate without an extra hydraulic circuit. In order to assure the highly stable operation, theoretical and experimental evaluation for initial friction coefficients, and seizure limits concerning with the pressure fluctuations due to the waviness and elastic deformation, are required.

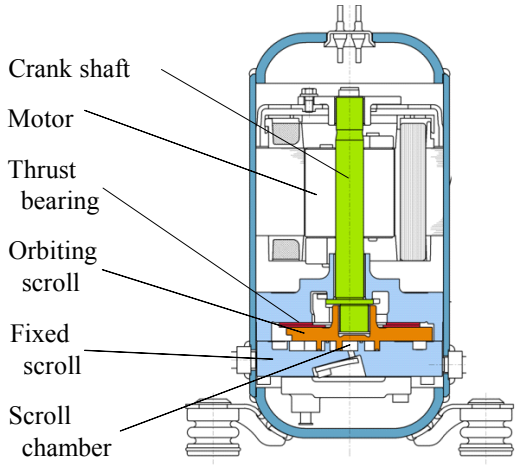

Fig. 1 Cross section of CO_2 scroll compressor

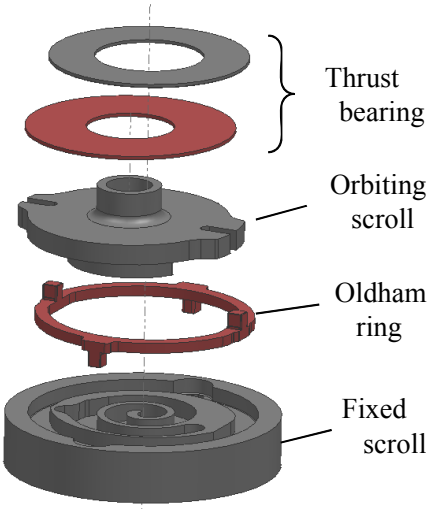

Fig. 2 Internal construction of scroll unit

Figure 2 shows the internal construction of the scroll unit. Fixed and orbiting scroll have the involute spiral. An eccentric crank shaft drives the upper scroll in an orbital motion, and an Oldham ring prevents its rotation.

In usual thrust sliding bearings, one of the surfaces rotates on the other mated surface. Some types of groove pattern is designed to facilitate hydrodynamic pressure generation and oil supply, concerning the rotational motion of the bearing. On the other hand, in case of the thrust bearing for scroll compressor, the moving surface does not rotate but only orbits in circle with the radius equal to the eccentric distance of the crankshaft. As the orbiting surface slides toward all directions, an axisymmetric local pattern is better for the orbital situation than rectilinear groove patterns. Some of the authors [3,4] proposed an embossed metal sheet for short stroke oscillatory slider, and named it "tribo-sheet". Experimental and theoretical results show that the geometrical wedge effect provides consistent and stable lubrication performance. This pattern is axisymmetric and suitable for the thrust bearing of scroll compressors.

Hamilton et al. [5] first proposed the lubrication mechanism of circular flat disk pattern and discussed on the role of outlet cavity formation. They treat the pattern as a step bearing and applied Reynolds equation to both of the top surface and groove area.

Figure 3 shows the proposed thrust bearing schematically. The lower flat plate is fixed to the orbiting scroll and slides on the upper patterned plate. Lubrication oil is supplied from inner circumference of the plate and dammed up by the outer seal ring. Filling oil fully into inter-bumps lubricate the top of the circular bumps.

As the hydrodynamic pressure and friction are mainly generated in the thin film area, the geometrical design of the top of the bump should be essential to control the frictional properties of the thrust bearing.

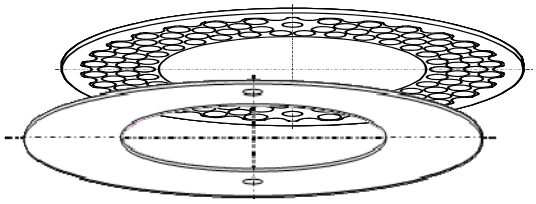

Fig. 3 Schematic view of thrust sliding bearing

Many of researchers have been reported the lubrication properties of pattered surfaces. Effects of the location and size of surface patterns are often discussed, but the qualitative effects of round off edge geometry of the flat base plane are merely considered.

We reported that the round off wedge profile generated by wear during initial running-in periods plays a dominant role of the lubrication performance of parallel sliders [6]. Looking at the industrial side of the bearing production, it would be desired that an optimum round off profile to demonstrate the maximum lubrication performance can be designed and elaborated without running-in process.

This study focused on the lubrication effects of a round off edge for axisymmetric circular patterns for thrust plate bearings. Elastohydrodynamic lubrication states of the idealized smooth surface model for the geometry of polished single pattern were examined by numerical EHL analysis. The practical frictional properties of the thrust plate with proposed lubricating pattern was examined experimentally. The seizure limits under extremely high loading conditions were also evaluated experimentally in consideration of unevenly distributed load due to the effects of initial waviness and elastic deformation of the orbiting scroll. These results show that the proposed pattern has sufficiently low friction over a wide range of operating conditions, and robustness against the accidental high loading.

2. Theoretical analysis and experimental

2.1. Numerical analysis

Figure 4 shows a typical model profile expressed by the power law formula,

$$z(r) = c\,(r/R)^m \,,\; r = \sqrt{x^2 + y^2} \,, \tag{1}$$

where c is the crowning height, R is the radius of the bump, r, x, y are radial and Cartesian coordinates, and m is the shape exponent which express the flatness or

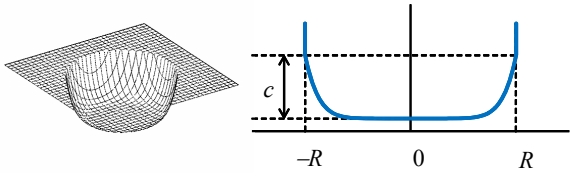

Fig. 4 Single bump model

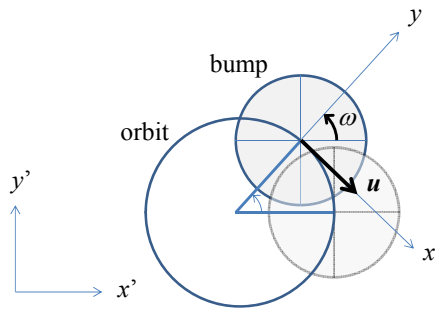

Fig. 5 Orbiting motion and coordinate system

the areal ratio of the corner wedge. This expression is often used to approximate the round off edge profile of polished surfaces and that after running-in. Spherical profiles are involved as the case $m=2$, that enables us to compare the results directly with well-known results of spherical EHL.

The orbiting motion of the flat slider can be decomposed into the translational velocity $\boldsymbol{u}$ and the rotational angular velocity ω as shown in Fig. 5. All of governing equations in this paper are defined on the local coordinates x, y. Except for the extra wedge effect due to the elastic deformation, the angular velocity term doesn't affect the lubrication state of the current axisymmetric profiles.

Governing equations are briefly summarized. The film equation, Reynolds equation, and the load balance equation are given as

$$h(\boldsymbol{x}) = h_0 + z(r) + \frac{2}{\pi E'} \iint \frac{p(\boldsymbol{x}')d\boldsymbol{x}'}{|\boldsymbol{x}-\boldsymbol{x}'|}, \tag{2}$$

$$\nabla \cdot \left(\frac{\rho h^3}{12\eta} \nabla p \right) = \boldsymbol{u}_m \cdot \nabla \rho h - \omega_m \, \boldsymbol{x} \times \nabla \rho h, \tag{3}$$

$$w = \iint p(\boldsymbol{x}) d\boldsymbol{x}, \tag{4}$$

with pressure $p(\boldsymbol{x}) = 0$ on the boundaries $r = R$.

Reynolds outlet boundary conditions for cavitation zone are assumed in numerical analysis and the pressure boundary conditions on $r = R$ mainly affects as the inlet boundary condition. As the bump radius is sufficiently large compared with the film thickness, the inlet boundary pressure should be almost zero. The effects of the inlet boundary condition were described in section 3.2.

2.2. Experimental for frictional properties

A schematic view of the experimental setup for the friction test is shown in Fig. 6. Each of the thrust sliding plates is fixed to the friction plate and the orbiting scroll. A set of the friction plate and the orbiting scroll is supported by the pair of thrust cross roller bearings. The lower thrust plate is driven with the drive plate by the crank shaft and the electric motor installed above the friction unit. A pair of plate springs is mounted on both side of the friction plate, and the translational friction force was measured as the average of the output from the strain gages on the plate springs. Representing friction values were obtained by the amplitude of measured sinusoidal waveforms. All of the components were assembled in the high pressure vessel and the axial load was supplied by the hydraulic unit. The gas pressure inside the high pressure vessel was controlled by the CO_2 refrigerant system and recirculating oil was supplied from the upper side of the vessel. The bumps are arrainged on the thrust plate in uniform inter-spacing as shown in Fig. 7. Sample geometry and experimental conditions are summarized in Table 1.

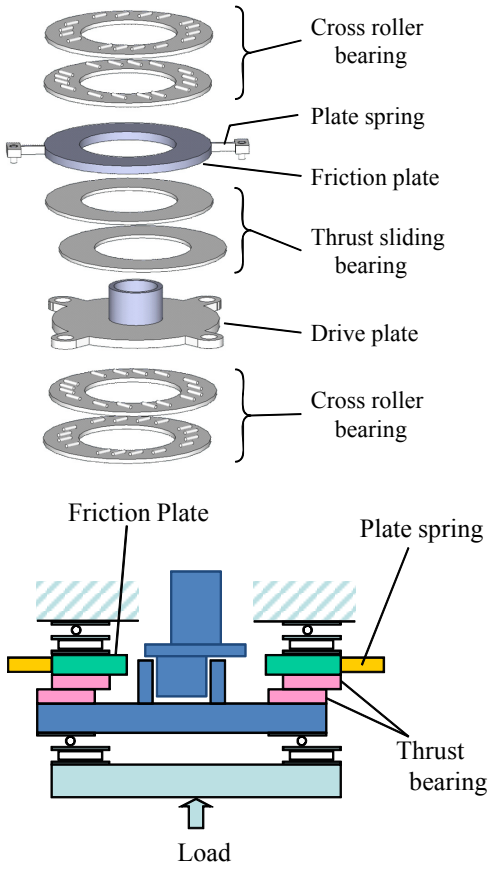

Fig. 6 Experimental setup for friction measurement

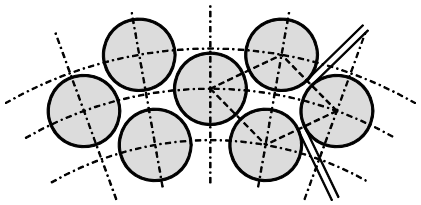

Fig. 7 Arrangement of the bumps

Table 1 Friction test sample and experimental condition

Thrust plate geometry

Material	hardened bearing steel
Outer diameter, [mm]	100
Inner diameter, [mm]	58
Thickness, [mm]	2

Bump geometry

Bump diameter, [mm]	4, 5, 5.5
Inter-bump spacing, [mm]	0.5
Number of bumps	176, 118, 106
Groove depth, [mm]	0.5
Crowning height, [μm]	0.5 to 30

Experimental condition

CO_2 gas pressure, [MPa]	3.8
Temperature, [^{0}C]	19
Viscosity, [mPa s]	5 to 7
Load, [N]	11 to 94 / bump
Sliding velocity, [m/s]	0.24 to 1.1

2.3. Experimental for seizure limits

Figure 8 shows an experimental setup for the seizure tests. A tri-islands specimen (Fig. 9) is held on the bottom of the oil bath, and a flat plate specimen rotates on it. Both of the samples are made of hardened bearing steel. In order to keep parallelism between the pair of the specimen, the oil pressure load is applied through the ball joint beneath the oil bath. Inside of the chamber is filled with CO_2 gas compressed at the pressure of 1MPa. As the CO_2 gas is absorbed to the lubricant oil and its pressure reduces in the initial period, a sufficient

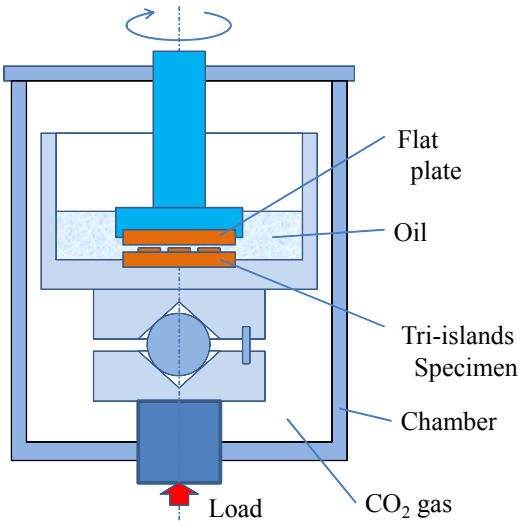

Fig. 8 Experimental setup for seizure tests

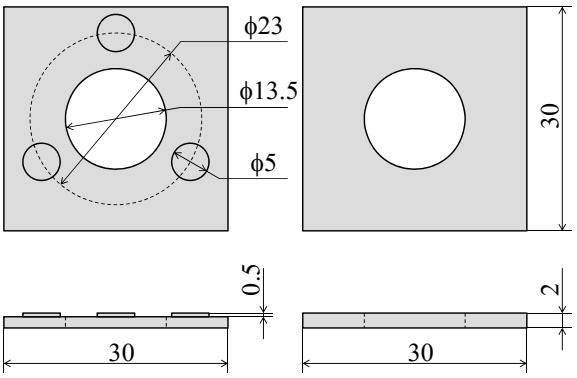

Fig. 9 A tri-islands specimen (left) and a flat plate specimen(right)

time to stabilize the gas pressure was taken before starting the tests. In order to handle a high load and large torque required to evaluate the seizure limits, the applied load was measured by the supplied oil pressure in the hydraulic cylinder and the frictional torque by the torsion bar on the lower shaft. Because these sensing units are mounted outside of the high pressure chamber, only the high frictional force in mixed lubrication regime was detected.

The seizure limits were evaluated under a constant increment rate of applied load (0 to 8 kN by 600 s) with constant sliding velocity (0.78 m/s). Frictional forces increased with increasing in applied load, and suddenly rose up after a period of unstable state. The seizure limit was defined by the applied load when the friction coefficient exceeds 0.3.

3. Results and discussion

3.1. Dimensional analysis

Ordinary, the numerical and experimental results are summarized in non-dimensional form. Traditionally, different kinds of non-dimensional expressions have been used for plain bearing theory, journal bearing theory, and EHL theory. In this paper, journal bearing type expression was used, which describes a lubrication state of fixed profiled bearings for given operating condition. The crowning height c in Eq.(1) was used for the characteristic length of the film thickness.

The dimensionless variables are defined as,

$$H=\frac{h}{c},\quad X=\frac{x}{R},\quad Y=\frac{y}{R},$$
$$P=\frac{pR^2}{w},\quad \bar{\mu}=\mu\frac{R}{c},\qquad (5)$$
$$G=\frac{\eta u_m R}{w},\quad S=G\left(\frac{R}{c}\right)^2.$$

Substitution in Reynolds equation Eq.(3),

$$\frac{\partial}{\partial X}\left(H^3\frac{\partial P}{\partial X}\right)+\frac{\partial}{\partial Y}\left(H^3\frac{\partial P}{\partial Y}\right)=12S\frac{\partial H}{\partial X}. \quad (6)$$

This expression has the same form to that of journal bearings. These expressions can be transformed to the expressions in pad bearings theory as follows,

$$\begin{aligned} K_w &= H_{\min}^2/S = \frac{w}{\eta_0 u_m R}\frac{h_{\min}^2}{R^2} \\ K_{\mu h} &\equiv \mu/(h_{\min}/R) = \bar{\mu}/H_{\min}, \\ K_{\mu w} &\equiv \mu/\sqrt{G} = \bar{\mu}/\sqrt{S} \end{aligned} \quad (7)$$

here, K_w denotes the load carrying capacity parameter, $K_{\mu h}$ and $K_{\mu w}$ denotes the friction coefficient parameters. Ordinary, these non-dimensional parameter is expressed as the function of the ratio between the inlet film thickness h_{in} and the outlet film thickness h_{out}. If the elastic deformation was sufficiently small, the relations $h_{out}=h_{\min}$, $h_{in}=c+h_{\min}$, and thus $(h_{in}/h_{out})=(1/H_{\min})+1$ are simply derived. Hereafter the factor $H_{\min}$ was also used as the control parameter for the non-dimensional parameters in Eq.(7).

3.2. Inlet boundary conditions

Figure 10 defines the boundary position of a single bump model. In most of the physical model, the pressure on the outer boundary is able to fix at zero. If the groove depth was thin against the horizontal size, Reynolds equation is applicable over whole area of analysis domain. Hamilton used this formulation. The groove of the scroll application is relatively deep and the Stokes flow analysis is required to determine the pressure profile in the groove area.

Reynolds outlet boundary conditions are assumed in numerical calculation, and the outlet boundary in Fig. 10 is placed inside the cavity area. In this case, the most important is the modeling of the inlet boundary. One of the possible modeling is the combined analysis with Stokes flow analysis in the groove area, and the other is

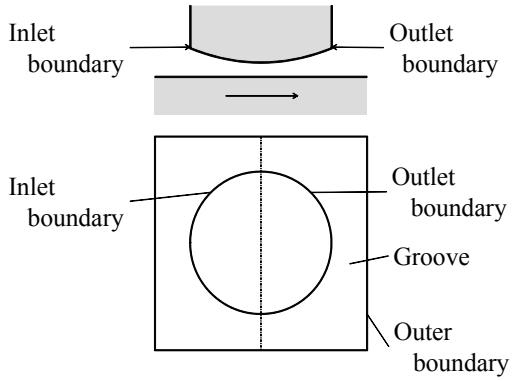

Fig. 10 Analysis domain and boundary conditions

the Reynolds equation based analysis for the bump geometry with sharp step profile.

Some of approximated formula for the inlet pressure are known in literature. The full-flooded condition of EHL is derived from Tipei's [9] potential flow analysis. The inlet pressure gradient is given by,

$$\frac{\partial p}{\partial x}=C_i\frac{\eta u_m}{h_i^2}, \quad (8)$$

where h_i is the film thickness at the inlet cavity boundary, $C_i=32/3$ for pure rolling and $C_i=4$ for pure sliding. Equating this result with Reynolds equation, full-flooded condition is given as,

$$\begin{aligned} &\text{pure rolling}: \quad (h_i/h_b)>9 \\ &\text{pure sliding}: \quad (h_i/h_b)>1.5 \end{aligned}. \quad (9)$$

Lakawatana [10] also analyzed the inlet pressure rise on a sharp corner edge. The pressure gradient is almost the same as Tipei's results for pure sliding and the inlet pressure rise is given by,

$$p_{inlet}=3.9\frac{\eta u_m}{h_b}, \quad (10)$$

where h_b is the film thickness on the sliding surface.

Assuming h_b was the order of $h_{\min}$, Eq. (10) and Eq. (7) gives the inlet pressure against the average lubricant pressure on the bump as,

$$p_{inlet}\frac{R^2}{w}=\frac{3.9}{K_w}\frac{h_{\min}}{R}. \quad (11)$$

As a result, if the bump size was large enough in relation to the minimum film thickness, the inlet pressure will never affect the total load support unless the load carrying capacity parameter was extremely small. In such a case, the inlet boundary pressure is able to fix at zero.

The inlet pressure is restricted by the reverse flow and consequent reduction of inlet flow due to the steeply expanded geometry. It can be called geometrical starvation.

Wide range calculation is desired to express the results in design charts. As discussed later, the effects of inlet boundary conditions only appear in high S regime. S factor is expressed by both of the operating condition G and aspect ratio (c/R). If the high speed or low load condition was supposed for large S regime, the film thickness will become thick and a step geometry modeling or full coupling with Stokes flow analysis is necessary. If the small (c/R) ratio of nominally flat bump profile was supposed, the zero inlet pressure approximation still holds. This study mainly considered the later situation.

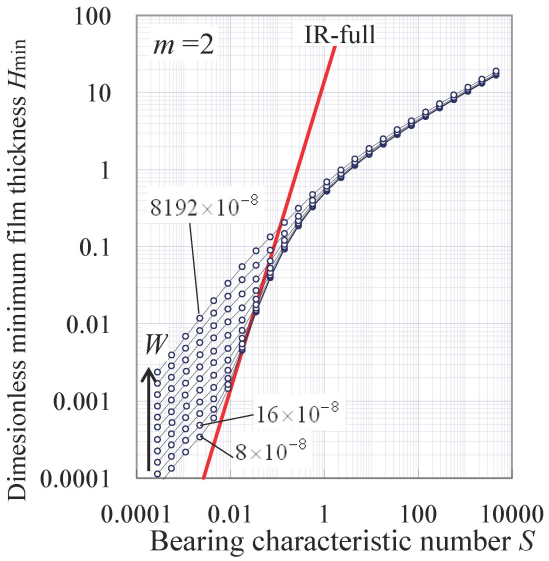

Fig. 11 Dimensionless minimum film thickness for m=2
[$W=(8,16,32,\ldots,8192)\times10^{-8}$]

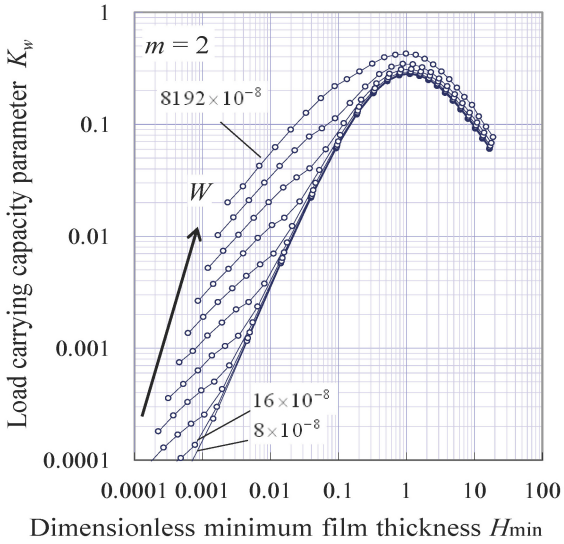

Fig. 12 Load carrying capacity parameter for m=2

3.3. Numerical EHL analysis

Figure 11 shows the dimensionless minimum film thickness for the case $m=2$. Here the load conditions are expressed by the non-dimensional parameter $W=w/E'R^2$. This case is spherical in shape, but the analysis area is limited to the radius R and the starvation effect is considered. In the lower S regime, minimum film thickness varies by the applied load due to its elastic deformation (iso-viscous elastic; IE regime). The lowest S part of the lines are located in the full-flooded regime, and their values are identical to that of standard EHL results. The strait red line shows the Kapitza's [8] analytical solution,

$$H_{\min}=(6\pi/5)^2 S^2, \qquad (8)$$

for full-flooded and iso-viscous rigid (IR) regime as reference. Here the relation $(R/c)=2$ for full-flooded spherical profile was used. The starvation effect appears as the reduction of $H_{\min}$ at higher S regime, and the inclination point are located at near-by $S\approx1$, otherwise $H_{\min}\approx1$.

As shown in the transformed diagram Fig. 12, the load carrying capacity parameter shows maximum at this inclination point ($H_{\min}\approx1$), that means the most effective crowning height is nearly equal to the minimum film thickness. The well-known optimum point of plain bearing is also placed at $H_{\min}\approx1$ ($h_{in}/h_{out}\approx2$), and this condition has a common physical meaning.

Figure 13 shows typical pressure profiles for low, middle and high $H_{\min}$ regime. As Fig.12 is a plain

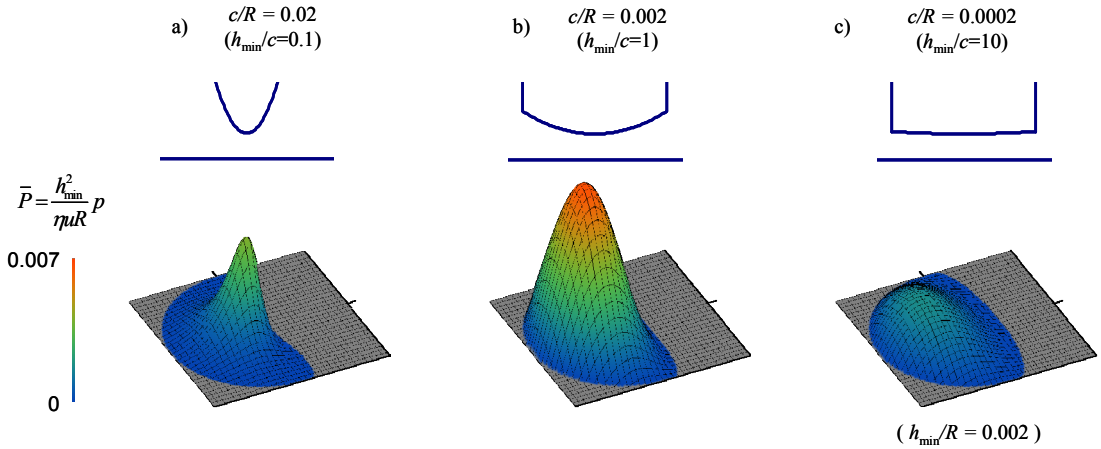

Fig. 13 Effects of aspect ratio on pressure profile

bearing type expression, these pressure was analyzed for a fixed minimum film thickness $(h_{\min}/R)=0.002$, and compared the results for the aspect ratios (c/R). Gray colored area indicates the cavitation or outside area of the bump, where the pressure is fixed at zero.

In low S and low $H_{\min}$ regime (Fig13 a), the fluid pressure arises only around the center of the bump and the most of the surface area doesn't contribute to the load support. This regime is a full-flooded regime and the inlet boundary condition doesn't affect the pressure profile. On the other hand, large S and $H_{\min}$ regime (Fig13 c), the pressure widely spreads over a bump, but the inlet flow is restricted by the starvation effect and the pressure level reduces. With increasing minimum film thickness, the tail of the oil pressure profile approaches the inlet boundary, and after the tail reached the boundary, the maximum pressure gradually restricted by starvation. Thus the slightly starved situation (Fig 13 b) gives the maximum load carrying capacity, where the relatively high oil pressure widely spreads over a bump.

In case of the higher load conditions in Fig. 12, the elastic deformation effect enhances a load carrying capacity parameter K_w and the maximum K_w point moves toward thin film thickness regime. This trend expresses the cooperative effect of starvation and elastic deformation. As well known for plain bearings, each of the friction coefficient parameters $K_{\mu h}$ and $K_{\mu w}$ has a minimum near by the maximum K_w point.

Figure 14 shows the results for the higher shape exponent ($m=8$). The slope of the $H_{\min}$ on S decreases compared to the spherical case, and the effects of elastic deformation is also reduces. This trend is explained as follows. By flattening the initial profile, the contact stiffness increases and the inlet film thickness also reduces. As a result, the load supporting area is enlarged and its load carrying capacity is improved. These flattening effects on the lubrication state are similar to that of elastic deformation.

As shown in Fig. 15 and 16, the maximum point of the load carrying capacity parameter and minimum point of friction coefficient parameter are still located at $H_{\min}\approx 1$. Load support effects of flat top profiles are suitable for thin film regime at severe operating conditions.

If the load was evenly supported by multiple bumps, the nominal applied load of scroll applications is relatively low, and majority of the bumps operate under IR regime. In order to describe the overall performance of the bearing, later discussion is focused on the starvation effects in IR regime.

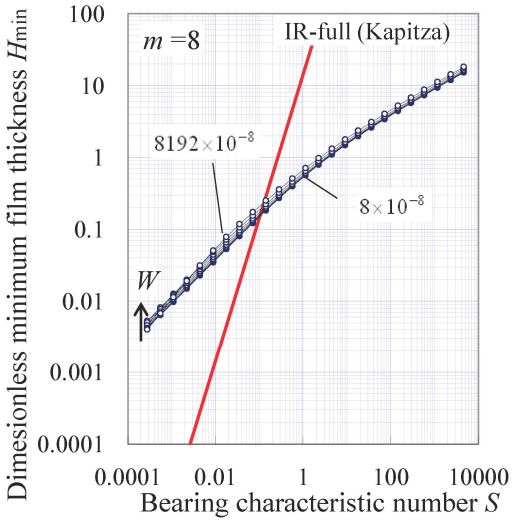

Fig. 14 Dimensionless minimum film thickness for m=8

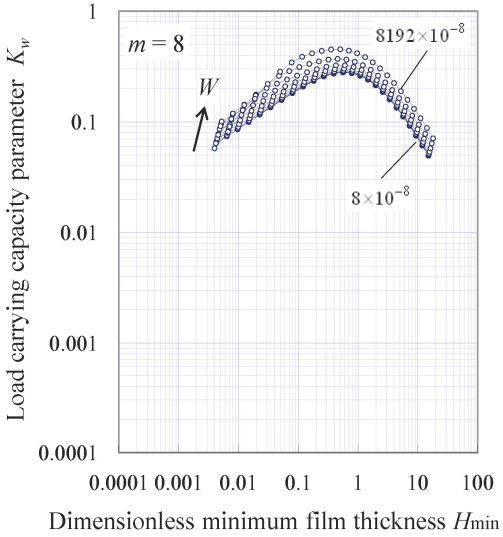

Fig. 15 Load carrying capacity parameter for m=8

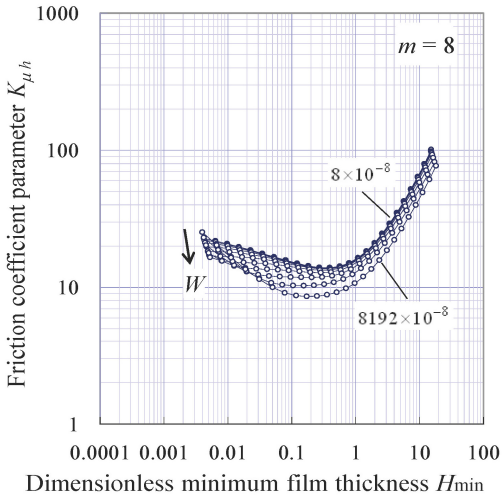

Fig. 16 Friction coefficient parameter for m=8

In Fig. 17 and 18, the dimensionless minimum film thickness and friction coefficient calculated for varied m were compared. The load condition is the minimum of the calculated range in Fig.11, where the elastic effects are negligibly small. Especially for the low S and thin film conditions, the minimum film thickness reduces for lower m. This thin film regime is stated at full-flooded condition and its oil pressure is concentrated around the center of the bump. In such a case, highly arched top causes a thinner film thickness. On the other hand, friction coefficients increases with m over all area, and this trend is explained as the effects of spreading frictional surfaces due to the flattening of the bump. In order to avoid the metal contact and reduce friction, middle range of $m \approx 10$ is optimum.

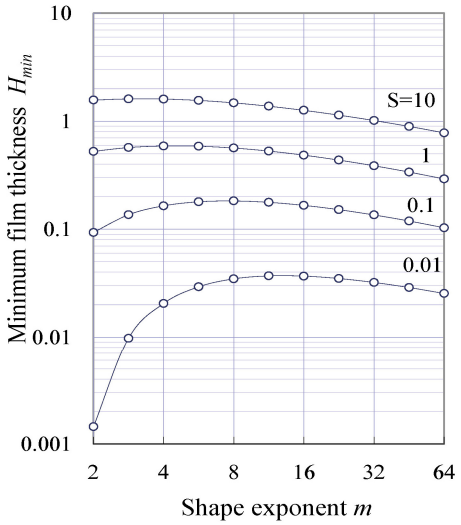

Fig. 17 Effects of m on minimum film thickness [$W = 8\times10^{-8}$]

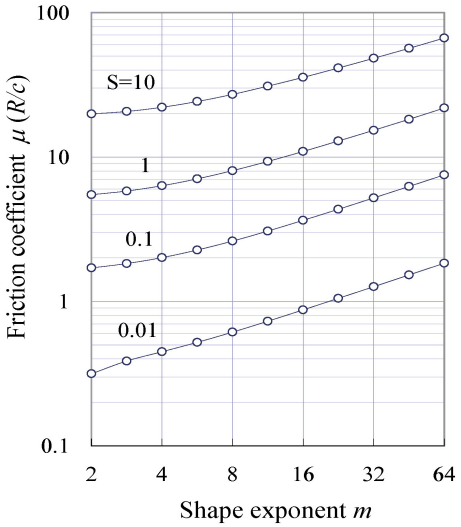

Fig. 18 Effects of m on friction coefficients [$W = 8\times10^{-8}$]

3.4. Experimental friction coefficients

Experimental conditions are expressed by the duty parameter G and theoretical optimum points are given by the bearing characteristic parameter S. These two parameters are combined with the aspect ratio (c/R). In order to validate the geometrical effects of the circular bumps, the friction coefficients of the thrust plates finished in various aspect ratios were experimentally evaluated.

The surface geometries of the finished plate were measured by a surface roughness meter and the geometrical parameters c, m were calculated by the height of sampling points. As shown in Fig. 19, there are the correlation between the crowning height c and the shape exponent m, where the large round off amount cases higher c and smaller m.

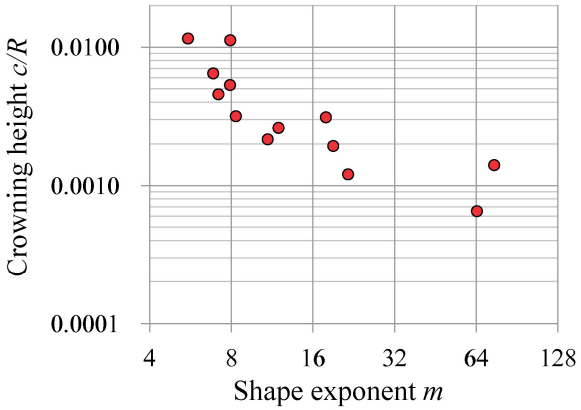

Fig. 19 Geometry factors of test samples

Figure 20 plots the evaluated friction coefficients for the duty parameter G, which represents the operating condition. The lubricant viscosity 5 mPa·s was assumed as lower estimation. In high velocity range (right hand side of Fig. 20), all of the samples show a trend to increase the friction with G, and its logarithmic slope is approximately 0.5. This trend is a feature of hydrodynamic lubrication regime in full-flooded condition. In low velocity conditions, the friction coefficient arise by reducing G, that shows the mixed lubrication effects appears. These friction coefficients were sufficiently small compared with the results for pattern-less flat plate pair.

These experiments were conducted from lowest sliding speed of 0.24 m/s to 1.1m/s in 5 steps, and the load was increased under each constant velocity. Except for the sample $c/R = 0.0115$, the friction curve traced on a single curve in mixed and hydrodynamic lubrication regime. This fact shows that the surface profile and surface roughness didn't change during the operation in mixed lubrication regime. Only the most pointed profile sample of $c/R = 0.0115$ shows the quite a high friction in the first set of the experiments and gradually reduced during later experiments. As a

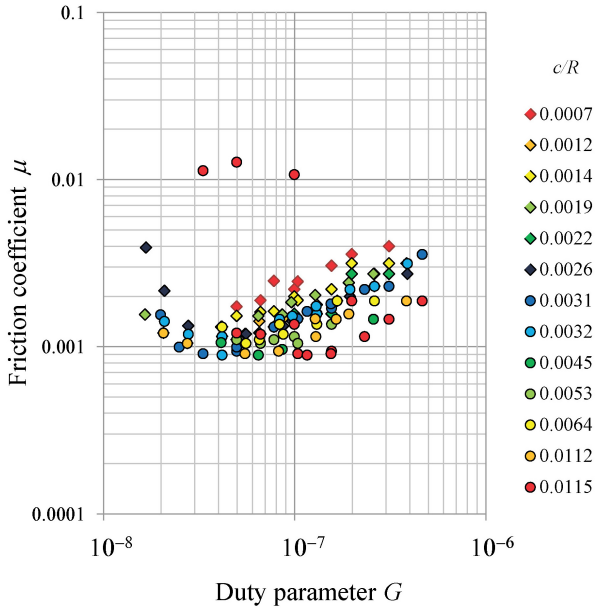

Fig. 20 Experimental friction coefficient

result, the friction coefficients for this sample plotted in separated 3 curves. This is considered that the top of the bump wore out during the operation under mixed lubrication regime.

Figure 21 shows the transformed diagram to the non-dimensional parameter sets, $S, \mu(R/c)$ which correct the effects of the crowning height. By introducing the measured crowning height of each sample, all of measured data in hydrodynamic lubrication state is able to express in single line.

The strait lines represent the numerically predicted friction coefficients for selected m. In this experiment, $m = 5$ and 21 denote the minimum and maximum value

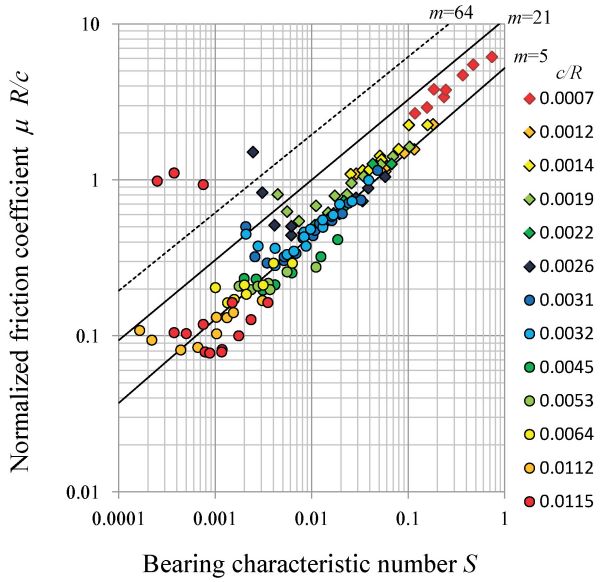

Fig. 21 Normalized friction coefficients comparing with numerical prediction

of exponent m of measured samples with the lower m value ($m < 32$), respectively, and $m = 64$ is arbitrarily-chosen large value. The predicted friction is slightly larger than the experiments, but differs only within a doubling.

As the parameter S corrects the crowning height effect by the factor (c/R), the results of highly arched samples with large (c/R) and small m are plotted on the left hand side of Fig. 21, and the flat samples with small (c/R) and large m on the right hand size. In the small m and highly arched bumps, the central film thickness is thin and the top the bump will wear out during the sliding in mixed lubrication. The result of maximum $c/R(=0.0115)$ seems to be separated in three lines. It is considered to be the effect of running-in wear during the series of experiments. This effect is one of the possible mechanisms of relatively low friction in low S range.

On the other hand, the surface profiles of the large m $(m>60)$ samples in high S range are nominally flat. In such a situation, unavoidable waviness effects will reduce the friction. Middle range of the geometry shows a relatively good agreement with experiments.

In comparison with the friction coefficients, the minimum film thickness is more sensitive on the lubrication state, because the friction coefficient is the averaged property over the sliding area, but the minimum film thickness is a local variable. In order to validate the numerically predicted minimum film thickness, the film parameter,

$$\Lambda = h_{\min}/\sigma, \tag{9}$$

was calculated using the combined roughness σ measured before testing, and the numerically predicted minimum film thickness $h_{\min}$ at the bearing characteristic number S on the minimum friction point in a series of experimental friction coefficients of a sample, upon the assumption that the minimum point addresses the starting S of mixed lubrication. Figure 22 shows the analyzed film parameters. Regardless of the sample geometry, all of the results is varied around $\Lambda \approx 3$, which is reasonable as the film parameter at a starting point of the mixed lubrication state.

Despite the simplicity of the single bump model based on a sampling geometry, the proposed model gives a physically consistent result and expresses the effects of crowning height and overall frictional properties.

3.5. Seizure limit

Under the normal applied load, relatively flat top profiles have a suitable load support by hydrodynamic lubrication effects, but if the extremely high load was applied, the pressure concentration due to the edge load should be considered.

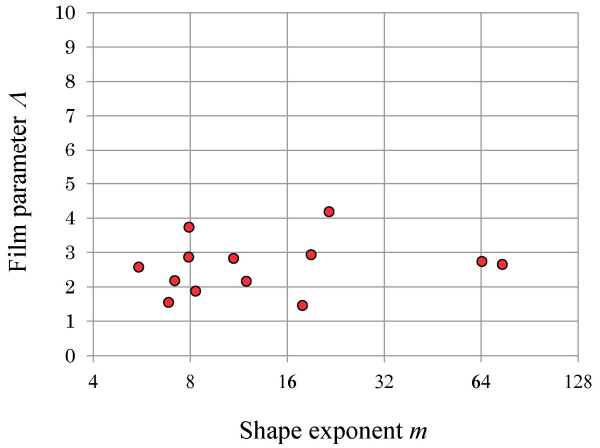

Fig. 22 Film parameter

In order to confirm the robustness against the fluctuation of the applied load of each bump due to the waviness of the thrust plates and global elastic deformation of compressor components, the seizure limit of a bump was evaluated by tri-island pattern sample shown in Fig. 9.

Figure 23 shows the evaluated seizure limits as the supportable maximum average pressure over the bump for the initial shape exponent m of the sample. The lower m group of the samples was finished by polishing, and the higher m group in the right-hand side of Fig. 23 is non-polished group.

The lowest seizure limit shown in Fig. 23 are still much higher than the possible maximum load of the compressor, but the seizure limits tend to reduce by sharp edge profiles.

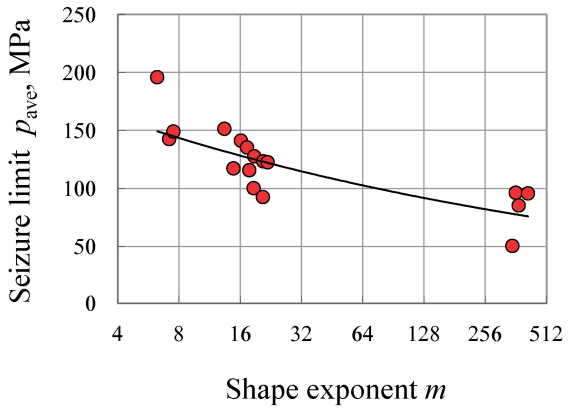

Fig. 23 Seizure test result

4. Conclusion

A thrust sliding bearing with a multiple circular bump pattern for a scroll compressor was proposed. The effects of the round off wedge profile of a bump were analyzed by elastohydrodynamic lubrication analysis. Based on the comparison with the experimental results, the following conclusions can be drawn:

1. General expressions independent from the aspect ratio of a bump can be derived by introducing non-dimensional parameters based on the crowning height.
2. The crowning height approximately equal to a minimum film thickness gives the maximum load carrying capacity and the minimum friction coefficient, where the bearing characteristic number is the order of 1. The latter condition gives an optimum aspect ratio of a bump.
3. The flattened top profile with large shape exponent assists the load support in thin oil film conditions, but enlarges the friction and slightly reduces the seizure limit.
4. The frictional properties of the proposed thrust bearing in hydrodynamic lubrication state are able to predict by the numerical analysis of a single bump model with considerable accuracy.
5. A transition to the mixed lubrication state is also predictable by comparing the surface roughness and the numerical minimum film thickness.

The proposed thrust bearing with multiple circular bumps shows a superior load carrying capacity and its frictional properties are controllable by the round-off wedge profile of crowning height and shape exponent.

Nomenclature

$z(r)$: un-deformed surface profile
c : crowning height
R : outer radius of the bump
m : shape exponent
x, y : Cartesian coordinates, $\boldsymbol{x}=(x,y)^T$
r, θ : cylindrical coordinates

ρ : density
η : viscosity
α : pressure viscosity index
E' : reduced elastic modulus
$(2/E')=(1-\nu_1^2)/E_1+(1-\nu_2^2)/E_2$
σ : combined roughness
$\sigma=\sqrt{\sigma_1^{\,2}+\sigma_2^{\,2}}$,
σ_1, σ_2 : root mean square roughness

$\boldsymbol{u}$: translational velocity $\boldsymbol{u}=(u_x,0)^T$
u_m : mean velocity $u_m=(u_{x1}+u_{x2})/2$
ω_m : mean angular velocity $\omega_m=(\omega_1+\omega_2)/2$

w : applied load
p : pressure
h : film thickness

h_0 : rigid displacement
$h_{\min}$: minimum film thickness
h_{in} : inlet film thickness
h_{out} : outlet film thickness
μ : friction coefficient

X, Y : dimensionless Cartesian coordinates $X = x/R, Y = y/R$
H : dimensionless film thickness $H = h/c$
P : dimensionless pressure $P = pR^2/w$
W : load parameter $W = w/(E'R^2)$
U : velocity parameter $U = (\eta_0 u_m)/(E'R)$
G : duty parameter (Lebeck[11,12]) $G = U/W$
S : bearing characteristic number $S = G(R/c)^2$
K_w : load carrying capacity parameter $K_w = H_{\min}^2/S$
$K_{\mu h}$: friction coefficient parameter $K_{\mu h} = \mu R/h_{\min}$
$K_{\mu w}$: friction coefficient parameter $K_{\mu w} = \mu/\sqrt{G}$
Λ : film parameter $\Lambda = h_{\min}/\sigma$

References

[1] Oku, T., Ishii, N., Anami, K., Sawai, K., Morimoto, T. and Iida, N., "An Optimal Performance Design on Lubrication Mechanism at Thrust Slide-Bearing of Scroll Compressors," Transactions of the JSRAE, 24, 3, 253-264 (In Japanese).

[2] Oku, T., Ishii, N., Anami, K., Knisely, C., Sawai, K., Morimoto, T. and Hiwata, A., "Theoretical Model of Lubrication Mechanism in the Thrust Slide-Bearing of Scroll Compressors," HVAC&R Research, 14, 2, 2008, 239-258.

[3] Nakamura, T., Matsubara, T., Itoigawa, F. and Nakamura, T., "Development of Tribo-Sheet Supporting Short-stroke Oscillatory Slide with Low Friction: Soft-EHL Analysis," JSME Annual Meeting III(01-1), 2001, 89-90 (in Japanese).

[4] Nakamura, T., Matsubara, T., Itoigawa, F., Hayakawa, S. and Yamada, T. , "Soft-EHL Analyses of Sliding Surface Structure and Development of Tribo-Sheet," Machine Design and Tribology Division Meeting in JSME, 2, 2002, 191-194 (in Japanese).

[5] Hamilton, D. B., Walowit, J. A. and Allen, C. M., "A Theory of Lubrication by Micro- Irregularities," ASME Journal of Basic Engineering, 88, 1, 1966, 177-185.

[6] Kawabata, S., Yoshida, K., Itoigawa, F. and Nakamura, T., "Transition of Surface Profile and Hydrodynamic Properties of Parallel Sliders under Running-In," Tribologists, 55, 2, 2010, 111-119 (In Japanese).

[7] Venner, C. H. and Lubrecht, A. A., "Multilevel Methods in Lubrication," Elsevier Science B.V., Amsterdam, 2000, 323-352.

[8] Kapitza, P. L., "Hydrodynamic Theory of Lubrication During Rolling," Zhurnal Tekhnicheskoi Fiziki, 25, 4, 1955, 747-762.

[9] Tipei, N., "Boundary Conditions of a Viscous Flow Between Surfaces With Rolling and Sliding Motion," ASME Journal of Lubrication Technology, 90, 1, 1968, 254-261.

[10] Lakawathana, P., Matsubara T. and Nakamura, T., "Mechanism of Hydrodynamic Load Capacity Generation on a Slideway", JSME International Journal, Series C, 41, 1, 1998, 125-133.

[11] Lebeck, A. O., "Parallel Sliding Load Support in the Mixed Friction Regime. Part 1 The Experimental Data," ASME Journal of Tribology, 109, 1987, 189-195.

[12] Lebeck, A. O., "Parallel Sliding Load Support in the Mixed Friction Regime. Part 2 Evaluation of the Mechanisms," ASME Journal of Tribology, 109, 1987, 196-205.